A REVIEW OF LAND COVER INFORMATION USING H/A/A POLARIMETRIC DECOMPOSITION OF DUAL POL SAR DATA

SUMAN SINHA

Department of Geography, Amity University Kolkata, Newtown, Kolkata, West Bengal, India.
Corresponding author email: sumanrumpa.sinha@gmail.com

ABSTRACT

Information related to land use and land cover is an inevitable prerequisite for formulating any decision making for land information system. The easiest and most effective way to gather such information is via using Earth observation satellites supported by ground data. Synthetic Aperture Radar (SAR), due to its additional unique intrinsic characteristics is favoured over the optical systems for procuring land information. An innovative and effective technique for land feature detection is the use of polarimetric capabilities of SAR. Generally applicable for quad polarized data, this study investigates the polarimetric capabilities of a dual polarized data obtained from ALOS PALSAR, which is not a general notion. The approach applied in the study shows accurate results for detection of land features using polarimetric decomposition of dual polarized ALOS PALSAR data over an area of Munger in the state of Bihar, India. Twelve distinct land cover features are identified in the study area using this approach. The polarimetric products are also investigated for deriving the biomass information for the vegetation cover in the study area. The relation between in-situ biomass generated from floral species-specific volumetric equations and SAR polarimetric products showed a moderate correlation of 0.56 with RMSE=29.13 t/ha and data agreement of 0.62 based on exponential regression model for predicting biomass. The decomposition parameters revealed more evidences for forest structure and feature identification rather than biomass information. The method adopted in the study can be well utilized for land resource information and mapping; hence, natural and man-made resource monitoring and management.

Keywords: SAR, ALOS PALSAR, polarimetric decomposition, LULC, biomass

INTRODUCTION

Forest being an important component of the carbon cycle reflects the state and health of our environment. The emerging climate change concept of reducing emissions from deforestation and forest degradation (REDD) comprises of the temporal change in the assessment of forest biomass/carbon stock (Sharma *et al.,* 2013). Above ground biomass (AGB) serves as the major carbon pool (Englhart *et al*., 2012). Successful implementation of REDD targets in the precise and accurate enumeration of biomass/carbon estimates (Sinha &

Santra, 2019). Development of forest inventories with field-generated measurements provides the most accurate means for AGB estimation using allometric equations (Sinha *et al.*, 2021).

In-spite of its high quality, the field-based method is arduous, time consuming, and difficult to apply in inaccessible areas with limited spatial information, which are prominent drawbacks in the assessment (Lu, 2006). In contrary, the ability of satellite remote sensing to cover extensive and remote areas made this technique a better approach for AGB estimation, however with lesser accuracy in the assessment in comparison to forest inventorization (Lu *et al.*, 2016).

The use of optical sensors for the forest structure (Chopping *et al.*, 2012), and biomass assessment (Kumar *et al.*, 2013), involves early saturation in the estimates, specifically for mature forests (Lu *et al.*, 2012: JFR). Thermal sensors too have limited use though relationship do exist between the surface temperature and biomass (Sinha & Sharma, 2013). Microwave synthetic aperture radar (SAR) sensor has the potential to give better estimates of biomass in comparison to optical sensors, due to its unique capability of canopy penetration leading to volumetric scattering and its interaction to surface roughness and moisture content even during adverse climatic conditions (Sinha *et al.*, 2015a). Recent studies reveal the importance of L-band SAR for forest biomass estimation due to its interaction with larger components of vegetation (Sinha *et al.*, 2019a, 2020a).

The range of retrievable AGB from L-band ALOS PALSAR data is 40–150 t/ha (Englhart *et al.*, 2011; Sinha *et al.*, 2016). Integrated use of multi-frequency SAR data have shown even better results (Sinha *et al.*, 2019b). Inability of the interferometric coherence information has led to the exploration of polarimetric decomposition analyses for forest biomass assessment (Sinha *et al.*, 2015b). Multi-polarized SAR data has great utility in land cover feature detection (Sinha *et al.*, 2020b). Polarimetry helps in image coherence decomposition to different scattering mechanisms and removes the azimuth slopes induced by the orientation angle (Sinha, 2016).

The distinct property of polarimetry adds to the potentiality of SAR that deals with the polarization state of the electromagnetic field. Polarimetric Synthetic Aperture Radar (PolSAR) advanced instrument used in remote sensing that plays an important role in understanding the electromagnetic phenomenology related to the complex targets and also the respective SAR image interpretation using the scattering mechanism of these complex targets (Gomathi *et al.*, 2021). Several coherent and incoherent target decomposition methods have been developed to understand these target-specific scattering mechanisms. H/A/α decomposition proposed by Cloude-Pottier helps in understanding the dichotomies of different targets (Kumar & Raghav, 2018). H/A/α decomposition of dual-pol SAR data simplifies the complex multi-parameter depolarization of quad-pol SAR data and reduces the high data processing requirement and storage issues. The improved Cloude-Pottier decomposition is widely used for segmentation and classification purposes (Ji & Wu, 2015). Dual polarized SAR data has wide ranged application, specially in land feature extractions (Sinha *et al.*, 2018a). The relatively easy data availability from spaceborne dual polarimetric SAR missions, like ASAR, Sentinel-1 and PALSAR with wider swath and greater temporal availability has more applicability (Potin *et al.*, 2014).

The use of models developed with polarimetric decompositions is mainly limited to image classification (Avtar *et al.*, 2011), rather than vegetation studies (Maity *et al.*, 2011) and biomass assessment (Tanase *et al.*, 2013). New SAR projects, for instance, NISAR (a collaborative project of NASA and ISRO) have been planned to explore the polarimetric capabilities, with a prime target of ecosystem-related studies including forest biomass estimation. Taking into consideration the urgency and importance of such technique, the

objective of this study is to investigate potential relationship between forest biomass with certain polarimetric scattering parameters (PSP) products generated from polarimetric target decomposition techniques and explore its capability to predict biomass.

MATERIALS AND METHODS

Study area and datasets

The study area of Munger forests is situated in the state of Bihar, India having geographic extent of 25º19'30"N–24º56'50"N latitudes and 86º33'33"E–86º11'51"E longitude as illustrated in Figure 1. Land use and land cover (LULC) analysis shows that nearly 89 % of the area is covered under forest out of which the dominant forest types are mixed; *Shorea robusta* (Sal), *Acacia catechu* (Khair) and *Dendrocalamus* sp. (Bamboo) forests. Munger forest division comprises reserved and protected forests of nearly 257.50 km² and 424.40 km² respectively; henceforth, the area under investigation comprises nearly 672.5 km² and the detailed LULC study of the area is performed (Sinha *et al*., 2013). Along with the survey of India (SOI) toposheets, ALOS PALSAR L-band dual HH/HV (FBD) polarized imagery dated 27th July, 2010 was used in the study. Details of the study site is mentioned in Sinha *et al*. (2013).

Fig. 1: Location of the study area
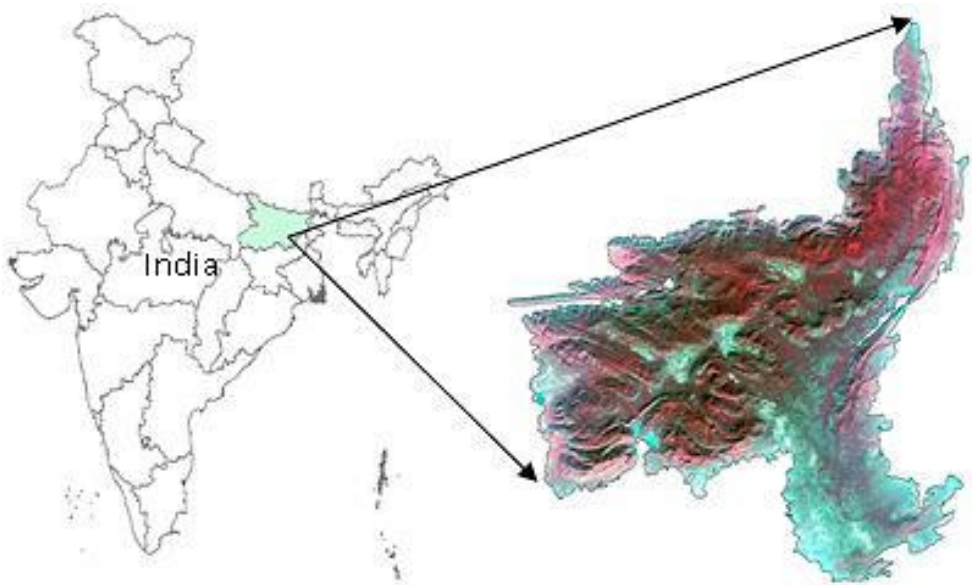
Methodology
Field Measurements

Field investigation was carried out to collect the training data during the same period of the SAR image acquisition. The training field data were used to establish the models for biomass estimation and serves as reference for SAR derived estimated biomass. Topographic sheets of 1:50,000 scale formed the base map for field inventory where a total of 45 square plots of 0.1 ha were laid from which primary data related to tree species name, height, girth at breast

height (GBH), diameter at breast height (DBH), etc. for all trees above 10 cm DBH were carried out. Out of the total 45 sample plots, 36 plots were randomly selected for model development whereas the remaining nine plots were used for model validation. Information regarding the geographic location (latitude/longitude) of the sample plots was recorded using global positioning system (GPS) and imported in GIS mode.

Field Estimation of Biomass

Standard procedure for biomass estimation using volumetric equation was followed (Sinha *et al.*, 2018b). For estimation of tree volume in the sample plots, local and general equations reported by forest survey of India were used. Tree GBH (converted to DBH) and tree height values were fed to the species-specific volumetric equations. The volume was then multiplied with specific gravity of the corresponding species to obtain biomass of individual trees. Individual tree biomass of all species in a plot was summed up to get biomass of the plot. This was done for all the 45 sample plots. The regional volumetric equation and specific gravity of major vegetation species type has been listed in Table 1. Here, V is the volume under bark (m^3), D is the diameter over bark at breast height (m), and H is the tree height (m); all measured in SI units.

Table 1: Volumetric equations and specific gravity for calculating biomass (FSI, 1996)
where, V=Volume under bark (m^3), D=Diameter at breast height (m), H= Tree height (m).

Botanical Name **	Volume Equation	Specific Gravity (ρ)
Acacia catechu	$V=0.21612–4.16597*D+24.50948*D^2-29.6773*D^3$	0.97
Adina cordifolia	$V=0.0052355+0.55615*D^2H$	0.62
Anogeissus latifolia	$V=0.020760+0.447658*D^2H$	0.89
Boswellia serrata	$V=2.091911*D+0.18818*D^2H–0.200382$	0.57
Buchanania lanzan	$V=0.017+0.381*D^2H$	0.56
Dendrocalamus strictus#	$\ln(AGB)=2.487+0.414*(\ln(\rho D^2H))$	1.1
Diospyros melanoxylon	$V=0.400004*D^2H–0.007336$	1.1
Madhuca latifolia	$V=0.275*D^2H–0.014$	0.94
Semecarpus anacardium	$V=(1.67477+14.83747*D–9.43386*\sqrt{D})^2$	0.62
Shorea robusta	$V=0.375132*D^2H–0.004092$	0.74
Sterculia urens	$V=0.27909–3.26515*D+13.46829*D^2$	0.57
Terminalia tomentosa	$V=0.42823*D^2H–0.002149$	0.84

** Nomenclature of the floral species are mentioned in FSI (1996).

SAR Polarimetric Decomposition

Polarimetric decompositions characterize the image in terms of its scattering mechanism. The two forms of decompositions: the coherent decomposition dealing with decomposition of the scattering matrix, and the incoherent decomposition dealing with decomposition of coherency or covariance matrices. In coherent decomposition, like Pauli decomposition, a single discrete scatterer produces a fully polarized wave.

The incoherent decomposition, H/A/α (entropy, anisotropy, alpha) decomposition uses coherency matrix, and coherent decomposition, Pauli decomposition technique uses scattering matrix expressed in Pauli basis were used in the study. Span gives the total power

22

received from all the polarimetric channels. Hence, the following major steps were undertaken:

- Scattering matrix,
- Covariance and coherency matrices,
- Polarimetric decomposition (Pauli and H/A/α decomposition), and
- Geocoding.

H/A/α decomposition was developed by Cloude and Pottier (Cloude & Pottier, 1997) using the second-order statistic-based smoothing algorithm (Gomathi *et al.*, 2021). Eigenvector analysis of the coherency matrix [T] involving the eigenvalues distribution and the characterization of the scattering mechanism, is used. Each feature on ground behaves as an unique scatterer and the process of scattering is analyzed through the decomposition using eigenvectors and their respective relative magnitudes using eigenvalues (Pottier *et al.*, 2008). The basics of polarimetric scattering mechanisms developed on a quad-pol data (Yonezawa *et al.*, 2012) needs to be modified for dual-pol data.

L-band is sensitive to the small surface variations as well as show penetration in the canopy layer (Sinha *et al.*, 2015a). Pauli images are in fact RGB images constructed from Pauli decomposition that necessitates the use of an orthogonal set of polarization data. Although, HH/HV is not an orthogonal set of data hence does not represent Pauli elements. Under monostatic conditions, the coherent decomposition of the scattering mechanisms is assessed by the Pauli decomposition. In this case, the PolSARPro software has been instructed and forced to generate polarimetric decompositions in order to visualize, investigate and interpret the outputs from the dual polarized data. Hence, the term 'PSRFBD False RGB composite' is used for Pauli RGB generated, simultaneously, the terms 'PSRFBD H/A/α and 'PSRFBD Span' is used for H/A/α decompositions and span respectively.

The general elements of the scattering matrix [S] for fully polarized SAR data are defined as

$$[S] = \begin{bmatrix} S_{HH} & S_{HV} \\ S_{VH} & S_{VV} \end{bmatrix} \quad (1)$$

The scattering matrix [S] for the HH/HV dual polarized (FBD) L-band ALOS PALSAR data is modified accordingly and expressed as

$$[S] = \begin{bmatrix} S_{HH} & S_{HV} \\ 0 & 0 \end{bmatrix} \quad (2)$$

The dual polarimetric mode has horizontal transmission and horizontal received in HH polarization, while horizontal transmission and vertical received in HV polarization. Hence, the corresponding scattering vector for the HH/HV dual polarimetric data can be expressed as

$$[S_{HH}\ 2S_{HV}]^T \quad (3)$$

T in eq. 3 refers to the transpose of matrix. Thereafter, the coherency matrix derived, and its decomposition can be represented in eqs. 4 and 5 respectively.

$$<T> = \frac{1}{L} \sum_{i=1}^{L} k_i k_i^H \quad (4)$$

$$<T> = \sum_{i=1}^{q} \lambda_i u_i u_i^H \quad (5)$$

where, L is the number of looks, k_i is the i th look of sample k (i =1, 2), H is the complex conjugate transpose, q is the number of polarized channels, λ_i is the eigen value of <T>, u_i is the eigen vector and <.> is the assembly average.

The averaged polarimetric scattering mechanism described by entropy H, alpha angle (α) and probabilities obtained from eigenvalues (anisotropy, A) is derived via POLSARPro based on the HH/HV dual polarized L-band SAR data.

'Span' gives the total power received from the four polarimetric channels. Span of [S] is expressed as $|S_{HH}|^2 + |S_{VV}|^2 + 2|S_{HV}|^2$ which is converted to $|S_{HH}|^2 + |S_{HV}|^2$ for HH/HV dual polarized data.

Fig. 2: Approach of the study
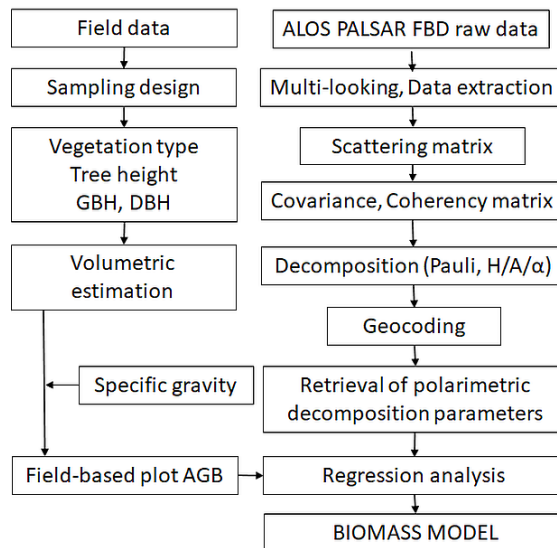
Biomass and PSP relationships

Figure 2 depicts the overall methodology for estimating AGB using SAR polarimetric decomposition using the ALOS PALSAR dataset. Remote sensing image processing software is used to extract the values of the polarimetric decomposition parameters and establish a relation between the polarimetric scattering parameters (PSPs) and the field-based plot AGB.

Regression Modeling

The model is generated from the 36 sample plot field-based data. The equation is used for calculating the biomass with information of Span as generated from the L-band ALOS PALSAR data and equated with the estimated 09 sample plot field-based data that are kept for evaluation of the model. The model is statistically validated with the nine additional field AGB data and the corresponding statistical measures that include coefficient of determination (R^2), root mean square error (RMSE), mean absolute deviation (MAD), mean bias error (MBE), non-dimensional RMSE (NDRMSE), non-dimensional MAD (NDMAD), non-dimensional MBE (NDMBE), average absolute accuracy (ς) and Willmott's index of agreement (*d*) are executed (Santra *et al.*, 2021; Sinha *et al.*, 2016).
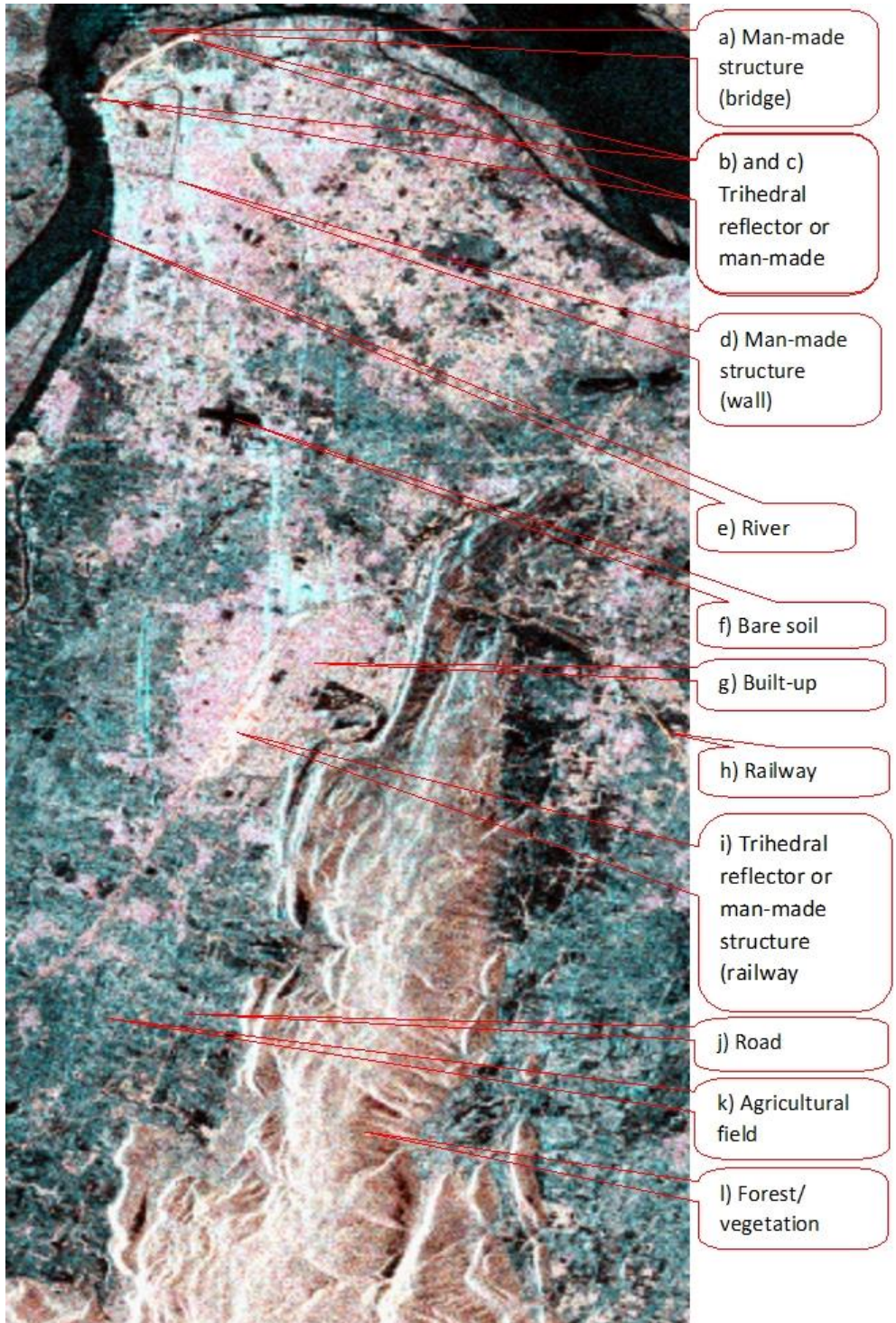
RESULTS

Field Measurements for AGB Estimation

Field-based AGB estimations showed the highest biomass accumulation for the *Shorea robusta* (sal) mixed forests of 172.07 t/ha (t/ha equivalent to Mg/ha) and thereafter for the mixed *Acacia catechu* (khair) forests with high density canopy cover. The minimum value of 11.35 t/ha occurred for the low density canopy cover of the *Acacia catechu* (khair), *Dendrocalamus* sp. (bamboo) mixed forests. The average and standard deviation (SD) of the AGB estimation value for all the plots was observed to be 72.94 and 41.15 t/ha respectively. The high SD indicates that the data points are spread out over a large range of values and the sample has large variation of data.

Fig. 3: PSRFBD False RGB composite of the study area

Fig. 4: Zoomed portion of PSRFBD False RGB composite

a) Man-made structure (bridge)

b) and c) Trihedral reflector or man-made

d) Man-made structure (wall)

e) River

f) Bare soil

g) Built-up

h) Railway

i) Trihedral reflector or man-made structure (railway

j) Road

k) Agricultural field

l) Forest/ vegetation

Fig. 5: Google Earth images identifying features from the zoomed portion mentioned in Figure 4

Polarimetric Analysis for LULC

The polarimetric decomposition analysis is used to identify the land cover features so as to separate the forest areas from the non-forested regions efficiently. The different scattering mechanisms occurring over the test study area shown by the PSRFBD False RGB composite is represented in Figure 3 and is specific for distinct features on ground. The figure shows an area marked in red that is zoomed in Figure 4 showing distinct land features. The following land features are identified: road, river, forest/vegetation, bare soil, built-up, man-made structures and agricultural fields. The Google Earth images of the features are shown in Figure 5 so as to visually compare the feature on ground as seen from high resolution satellite image to that obtained as signatures from PSRFBD False RGB composite image. On the other hand, Figure 6 shows the PSP products generated in the area. Most of the forested areas show that α values, depicting the dominant scattering mechanism, lie within the range of 0 to 45°. The values show a very weak correlation with the plot AGB (Figure 7). The figure also

shows that the value ranges within 10–30° for the selected sample plots. The value of H ranges from 0.5 to 0.9 for the selected sample plots which indicates depolarizing system of scatterers and scattering is from the mixture of point scatterers. However, there exist a very poor relationship between the plot AGB and the H as illustrated in Figure 7. Polarimetric scattering anisotropy (A) is the parameter complementary to H. It shows poor correlation with the plot AGB, however, at H>0.7, it shows better correlation (Figure 7). Span, which is a measure of total scattered power, shows the best relationship. Eq. (6) is developed from the relation between plot AGB with:

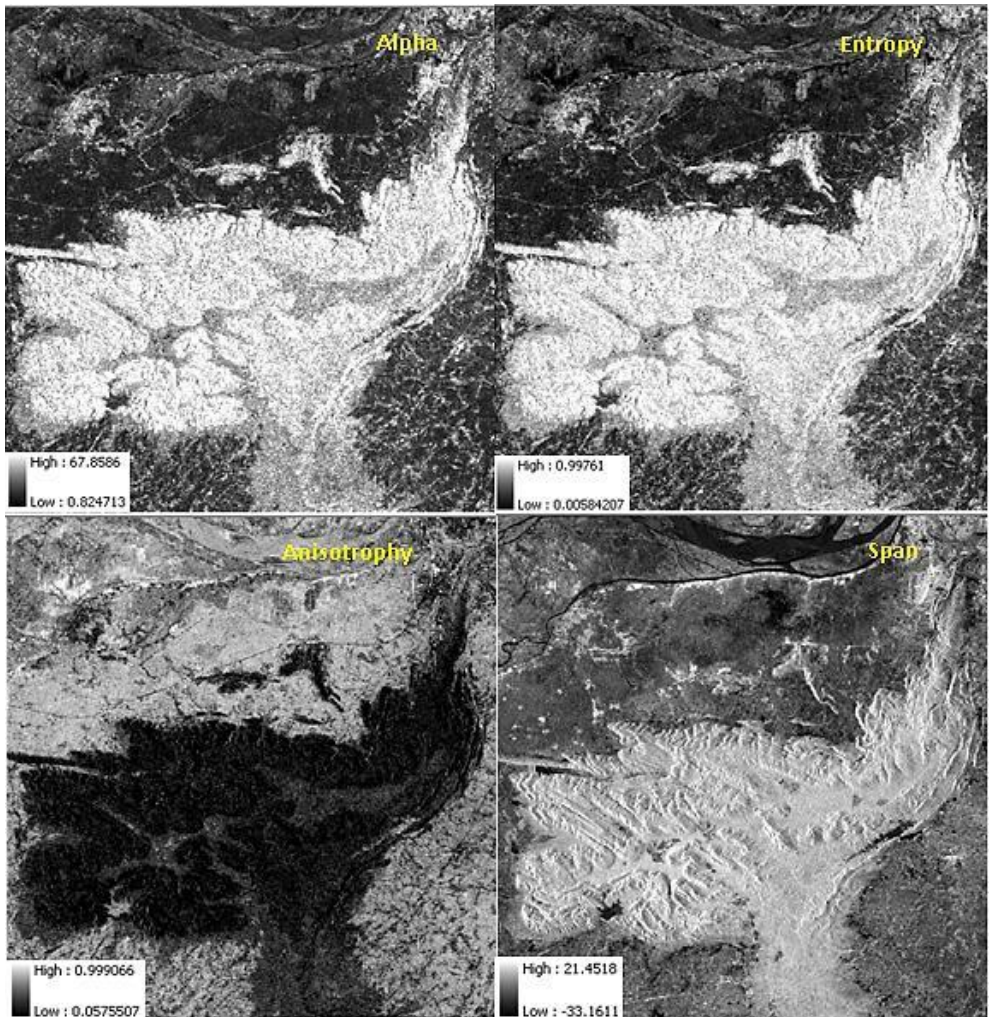$$AGB = 120.5 * e^{(0.063*Span)} \tag{6}$$
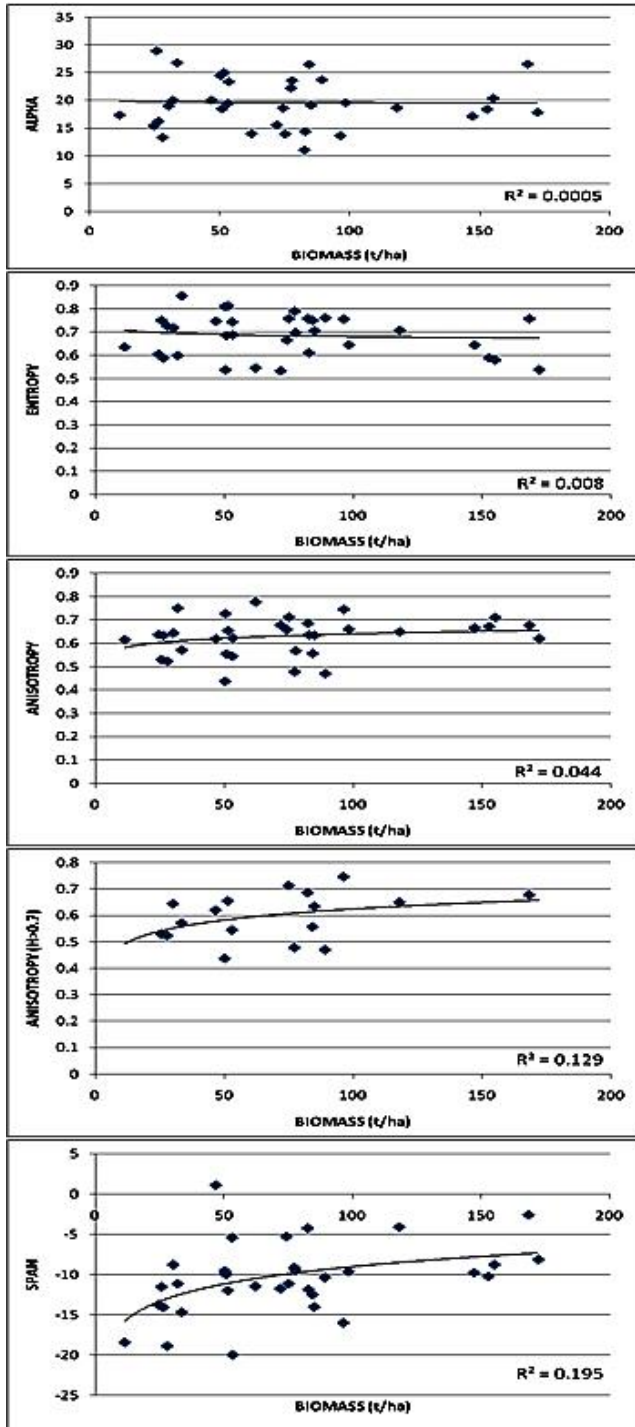
Fig. 6: PSP parameters

Fig. 7: Relationship between Plot AGB and PSPs

AGB Calculation

The Eq. (6) is generated from the 36 sample plot field-based data used for developing the biomass model. The model is statistically validated with nine additional field AGB data and evaluated. Table 2 documents the results of model evaluation and Figure 8 represents the graph between the predicted and estimated AGB values. Results showed the agreement for model validation is 0.622, with R2 of 0.565 and RMSE 29.136 t/ha. This reveals the potential of polarimetric span in the estimation of AGB. The biomass map developed from Eq. (6) is shown in Figure 9, which shows the spatial extent of the distribution of AGB over the study area.

Table 2: Model Evaluation Statistical Parameters

R^2	RMSE (t/ha)	NDRMSE	MAD	NDMAD	MBE	NDMBE	Slope	Av. Abs. Accuracy	Willmott's Index (*d*)
0.565	29.136	1.489	25.316	0.763	16.326	0.683	0.323	23.692	0.622

Fig. 8: Predicted vs estimated values
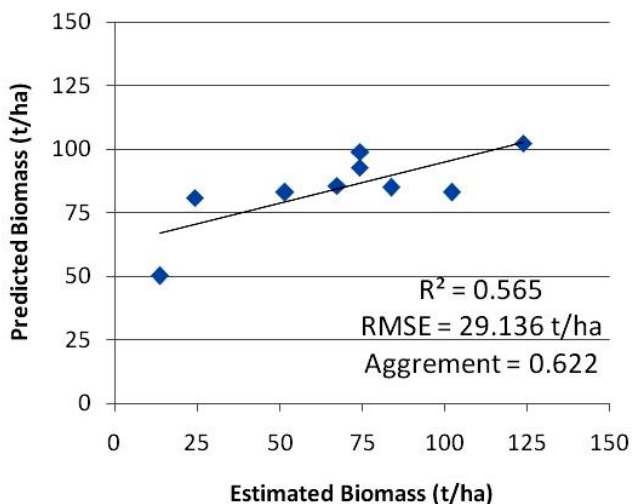
Fig. 9: Above-ground biomass map
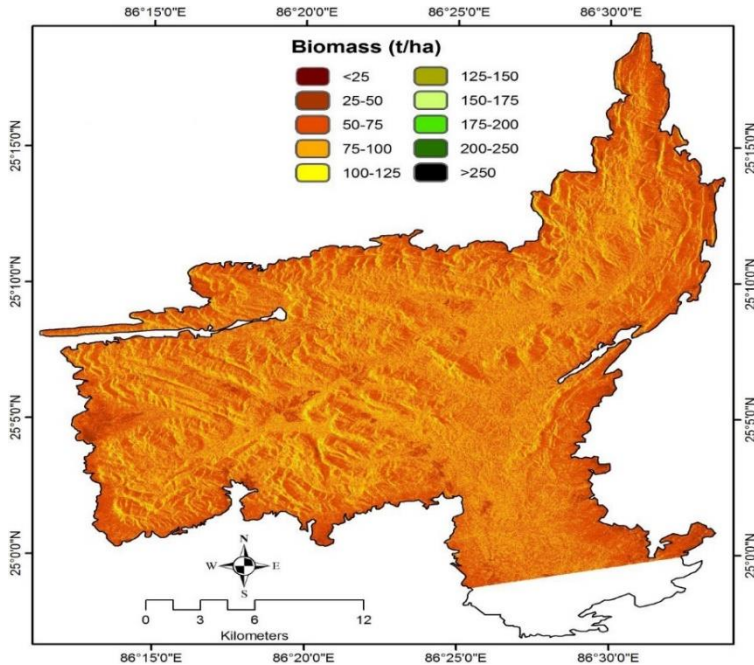
DISCUSSION

Polarized decomposition for LULC

Scattering mechanisms vary with different land features. Referring to figures 3 and 4, in this study area, dominated by open sparse and degraded forests, the brownish-red color represents double-bounce scattering from tree trunk-ground interactions. Pink color of the built-up areas results from a mixture of double-bounce and odd-bounce scattering. River is demarcated in dark-blue represents surface (odd-bounce) scattering. Cyan color represents a mixture from odd-bounce and volume scattering from the agricultural fields; however, odd-bounce scattering seems to have more contribution. Bare soil is symbolized in black color due to lack of any scattering and L-band with high penetration power penetrates the ground. The linear features like road, wall, bridge, etc. are clear from the figure. The figure shows high backscatter from the trihedral reflector caused by the odd bounce scattering, mostly observed at the railway junctions. The Google Earth images of the features are shown in Figure 5 so as to visually compare the feature on ground as seen from high resolution satellite image to that obtained as signatures from PSRFBD False RGB composite image. This reveals that there exist specific signatures for every land features depending upon the scattering mechanisms that the features undergo. Hence, the signatures should also vary depending on the tree structure and orientation in a forest. After clearly demarcating every pixel under forest or non-forest class, investigation for forest above-ground biomass is done on the forest pixels.

Polarimetric Scattering Parameters

Alpha (α) is the roll invariant parameter, depicting the dominant scattering mechanism is associated with the physics behind the scattering process involved (Agashe, 2013). The value ranges between 0 and 90°. α value represents the following mechanisms:

1. α=0° represents isotropic odd bounce scattering or surface scattering where the surface roughness variation is larger than the wavelength of incident wave.
2. 0°≤α≤45° represents anisotropic odd bounce scattering or surface where the surface roughness variation is smaller than the wavelength of incident wave.
3. α=45° represents Bragg surface model, like the dipole or volume scattering by cloud of anisotropic particles.
4. 45°≤α≤90° represents anisotropic even or multiple bounce scattering, like scattering from two perpendicular dielectric surfaces.
5. α=90° represents isotropic even or multiple bounce scattering, like the reflection from two perpendicular metallic surfaces.

Polarimetric scattering entropy (H) is a roll invariant parameter measuring the statistical disorder of each different scatterer within the group. The value of H indicates the type of scatterers.

1. H=0 indicates a single scattering mechanism.
2. A low value of H (H<0.3) indicates scattering from a dominant scatterer and the system is considered to be weakly depolarizing.
3. A high value of H (H>0.3) indicates depolarizing system of scatterers and scattering is from the mixture of point scatterers.
4. H=1 indicates random target scattering process representing completely depolarizing system.

Polarimetric scattering anisotropy (A) is the parameter complementary to H. It becomes a valuable parameter particularly when H attains a high value. Low H values give noisy anisotropy. As the value of H increases (H>0.7), it becomes difficult to distinguish between different types of scattering processes involved. At this point, anisotropy becomes useful for identification of the number of distinguishable scattering processes (Agashe, 2013). PSPs imparted more information regarding forest structure rather than providing information on biomass; yet the PSPs showed potential in enumerating the forest biomass; specifically, the 'Span' component.

CONCLUSIONS

Polarimetry in SAR provides new opportunity in the field of remote sensing of forestry. Of all the wave polarizations, HH and HV polarizations provide maximum information regarding tree biomass. The choice of ALOS PALSAR (FBD) HH/HV dual polarization dataset is hence accurate for the study. Relationship between ground biomass and corresponding PSP products is investigated and a biomass estimation model is developed based on linear regression analysis of the maximally correlated PSP, which is span, as observed in this study. The model developed on 36 sample points and validated on additional nine points showed R2 = 0.565 with RMSE = 29.13 t/ha and Willmott's index of agreement of 0.62. PSPs imparted more information regarding forest structure rather than providing information on biomass; yet the PSPs showed potential in enumerating the forest biomass. The performance of the model can potentially improve by developing more sophisticated models involving ground topography, soil moisture and forest structure and using fully

polarized SAR data. The study showed that not even quad pol data is required to efficiently demarcate the land features as in many cases, quad pol data is not available, rather dual pol data is relatively easier to obtain, especially with the advent of Sentinel. Henceforth, the approach can be easily applied over other regions in all scales to retrieve land and biomass information with accuracy. Hence, the study can augment forestry, climate change and REDD research, simultaneously overcoming the limitations offered by traditional field-based and conventional optical sensor-based biomass estimation approaches.

CONFLICTS OF INTEREST

The authors declare no conflict of interest.

REFERENCES

Agashe, S. (2013). *Polarimetric Decomposition of SAR Data for Forest Structure Assessment*. M.S. Dissertation, Dept. Earth and Space Sciences, Chalmers University of Technology, Göteborg, Sweden.

Avtar, R., Takeuchi, W., and Sawada, H. (2011). Full polarimetric PALSAR-based land cover monitoring in Cambodia for implementation of REDD policies. *International Journal of Digital Earth*, 6 (3), 255–275. DOI:10.1080/17538947.2011.620639.

Chaturvedi, R.K., Raghubanshi, A.S. and Singh, J.S. (2012). Biomass estimation of dry tropical woody species at juvenile stage. *The Scientific World Journal*, 2012, 1-5. DOI:10.1100/2012/790219.

Chopping, M., North, M., Chen, J., Schaaf, C.B., Blair, J.B., Martonchik, J.V. and Bull, M.A. (2012). Forest canopy cover and height from MISR in topographically complex Southwestern US landscapes assessed with high quality reference data. IEEE *Journal of Selected Topics in Applied Earth Observations and Remote Sensing,* 5 (1), 44-58. DOI:10.1109/JSTARS.2012.2184270.

Cloude, S.R and Eric, Pottier E. (1997). An Entropy Based Classification Scheme for Land Applications of Polarimetric SAR. *IEEE Transactions on Geoscience and Remote Sensing*, 35 (1), 68-78. DOI:10.1109/36.551935.

Englhart, S., Keuck, V. and Siegert, F. (2011). Aboveground biomass retrieval in tropical forests - the potential of combined X- and L-band SAR data. *Remote Sensing of Environment*, 115, 1260-1271. DOI:10.1016/j.rse.2011.01.008.

Englhart, S., Keuck, V. and Siegert, F. (2012). Modeling aboveground biomass in tropical forests using multi-frequency SAR data – a comparison of methods. IEEE *Journal of Selected Topics in Applied Earth Observations and Remote Sensing*, 5, 298-306. DOI:10.1109/JSTARS.2011.2176720.

FSI, (1996). *Volume Equations for Forests of India, Nepal and Bhutan.* Forest Survey of India, Ministry of Environment and Forests, Government of India, Dehradun. India.

Gomathi, M., Geetha, Priya, M., Chandre Gowda, C. and Krishnaveni, D. (2021). Flood damage assessment using H-A-Alpha dual polarimetric decomposition for Godavari Flood-2019. In: Komanapalli, V. et al. (eds.), *Advances in Automation, Signal Processing, Instrumentation, and Control, Lecture Notes in Electrical Engineering* (pp. 1199-1208), 700. DOI:10.1007/978-981-15-8221-9_113.

Ji, K. and Wu, Y. (2015). Scattering mechanism extraction by a modified Cloude-Pottier

decomposition for dual polarization SAR. *Remote Sensing*, 7 (6), 7447–7470. DOI:10.3390/rs70607447.

Kumar, A.R. and Raghav, A.A. (2018). A case study on the flood situation of Assam state. *International Research Journal of Engineering and Technology*, 5 (5), 4192–4194.

Kumar, P., Sharma, L.K., Pandey, P.C., Sinha, S. and Nathawat, M.S. (2013). Geospatial strategy for tropical forest-wildlife reserve biomass estimation. *IEEE Journal of Selected Topics in Applied Earth Observations and Remote Sensing,* 6 (2), 917-923. DOI:10.1109/JSTARS.2012.2221123.

Lu, D. (2006). The potential and challenge of remote sensing-based biomass estimation. *International Journal of Remote Sensing*, 27 (7), 1297-1328. DOI:10.1080/01431160500486732.

Lu, D., Chen, Q., Wang, G., Liu, L., Li, G. and Moran, E. (2016). A survey of remote sensing-based aboveground biomass estimation methods in forest ecosystems. *International Journal of Digital Earth,* 9 (1), 63-105. DOI:10.1080/17538947.2014.990526.

Maity, S., Patnaik, C., Parihar, J. S., Panigrahy, S. and Reddy, K.A. (2011). Study of physical phenomena of vegetation using polarimetric scattering indices and entropy. *IEEE Journal of Selected Topics in Applied Earth Observations and Remote Sensing*, 4 (2), 432-438. DOI:10.1109/JSTARS.2010.2076272.

Potin, P., Rosich, B., Roeder, J., and Bargellini, P. (2014). Sentinel-1 Mission operations concept. In: *IEEE Geoscience and Remote Sensing Symposium* (pp. 1465–1468), 13-18 July 2014, Quebec City, QC, Canada. DOI:10.1109/IGARSS.2014.6946713.

Pottier, E., Lee, J.S. and Ferro-Famil, L. (2008). *Advanced concepts*, PolSARpro v3.0 - Lecture Notes.

Santra, A., Mitra, S.S. and Sinha, S. (2021). Estimation and counter- validation of LISS-III derived leaf area index in Deltaic vegetation. *Caspian Journal of Environmental Sciences*, 19 (2), 239-249. DOI:10.22124/CJES.2021.4741.

Sharma, L.K., Nathawat, M.S. and Sinha, S. (2013). Top-down and bottom-up approach for above ground forest biomass and carbon monitoring in REDD framework using multi-resolution satellite data. *Environmental Monitoring and Assessment*, 185 (10), 8621-8637. DOI:10.1007/s10661-013-3199-y.

Sinha, S. (2016). Polarimetric Scattering Parameter products of ALOS PALSAR for forest biomass assessment. *Research & Reviews*: *Journal of Space Science & Technology*, 5 (1), 1-9.

Sinha, S. and Santra, A. (2019). An estimation of change in forest above ground carbon in Bhimbandh Wildlife Sanctuary between 2007 and 2016. *Current Science*, 117 (6), 1090-1094. DOI:10.18520/cs/v117/i6/1090-1094.

Sinha, S. and Sharma, L.K. (2013). Investigations on potential relationship between biomass and surface temperature using thermal remote sensing over tropical deciduous forests. *Research & Reviews: Journal of Space Science & Technology*, 2 (3), 13-18.

Sinha, S., Jeganathan, C., Sharma, L.K. and Nathawat, M.S. (2015a). A review of radar remote sensing for biomass estimation. *International Journal of Environmental Science and Technology*, 12, 1779-1792. DOI:10.1007/s13762-015-0750-0.

Sinha, S., Jeganathan, C., Sharma, L.K., Nathawat, M.S., Das, A.K. and Mohan, S. (2016). Developing synergy regression models with space-borne ALOS PALSAR and Landsat TM sensors for retrieving tropical forest biomass. *Journal of Earth System Science*, 125 (4), 725-735. DOI:10.1007/s12040-016-0692-z.

Sinha, S., Mohan, S., Das, A.K., Sharma, L.K., Jeganathan, C., Santra, A., Mitra, S.S. and Nathawat, M.S. (2020a). Multi-sensor approach integrating optical and multi-frequency synthetic aperture radar for carbon stock estimation over a tropical deciduous forest in India. *Carbon Management*, 11 (1), 39-55. DOI:10.1080/17583004.2019.1686931.

Sinha, S., Santra, A. and Mitra, S.S. (2020b). Semi-automated impervious feature extraction using built-up indices developed from space-borne optical and SAR remotely sensed sensors. *Advances in Space Research*, 66 (6), 1372-1385. DOI:10.1016/j.asr.2020.05.040.

Sinha, S., Santra, A. and Mitra, S.S. (2018a). A method for built-up area extraction using dual polarimetric ALOS PALSAR. *ISPRS Annals of the Photogrammetry, Remote Sensing and Spatial Information Sciences*, IV-5, 455-458. DOI:10.5194/isprs-annals-IV-5-455-2018.

Sinha, S., Santra, A., Das, A.K., Sharma, L.K., Mohan, S., Nathawat, M.S., Mitra, S.S. and Jeganathan, C. (2019a). Accounting tropical forest carbon stock with synergistic use of space-borne ALOS PALSAR and COSMO-Skymed SAR sensors. *Tropical Ecology*, 60, 83–93. DOI:10.1007/s42965-019-00011-6.

Sinha, S., Santra, A., Das, A.K., Sharma, L.K., Mohan, S., Nathawat, M.S., Mitra, S.S. and Jeganathan, C. (2019b). Regression-based integrated bi-sensor SAR data model to estimate forest carbon stock. *Journal of the Indian Society of Remote Sensing*, 47, 1599–1608. DOI:10.1007/s12524-019-01004-7.

Sinha, S., Santra, A., Sharma, L.K., Das, A.K., Jeganathan, C., Mohan, S. and Mitra, S.S. (2021). Responses of Multi-Frequency Remote Sensing to Forest Biomass. In: Pandey P.C., Sharma L.K. (eds) *Advances in Remote Sensing for Natural Resource Monitoring* (pp. 58-80). John Wiley & Sons, UK. DOI:10.1002/9781119616016.ch5.

Sinha, S., Santra, A., Sharma, L.K., Jeganathan, C., Nathawat, M.S., Das, A.K. and Mohan, S. (2018b). Multi-polarized Radarsat-2 satellite sensor in assessing forest vigor from above ground biomass. *Journal of Forestry Research*, 29 (4), 1139-1145. DOI:10.1007/s11676-017-0511-7.

Sinha, S., Sharma, L.K. and Nathawat, M.S. (2013). Integrated geospatial techniques for land-use/land-cover and forest mapping of deciduous Munger forests (India). *Universal Journal of Environmental Research and Technology*, 3 (2), 190-198.

Sinha, S., Sharma, L.K., Jeganathan, C., Nathawat, M.S., Das, A.K. and Mohan, S. (2015b). Efficacy of InSAR coherence in tropical forest remote sensing in context of REDD. *International Journal of Advancement in Remote Sensing, GIS & Geography*, 3 (1a), 38-46.

Tanase, M.A., Panciera, R., Lowell, K., Hacker, J. and Walker, J.P. (2013). Estimation of forest biomass from L-band polarimetric decomposition components. In Proc. *IEEE Geoscience and Remote Sensing Symposium (IGARSS)* (pp. 949-952), 2013, Melbourne, VIC. DOI:10.1109/IGARSS.2013.6721318.

Yonezawa, C., Watanabe, M. and Saito, G. (2012). Polarimetric decomposition analysis of ALOS PALSAR observation data before and after a landslide event, *Remote Sensing* 4, 2314-2328. DOI:10.3390/rs4082314.